ORNL/TM-2023/2883

CRADA Final Report - NFE-19-07946 Development and testing of residential micro-CHP powered by opposed piston engine

Zhiming Gao
Philip Zoldak
Jonathan Mansinger
Joseph DeMaria
Tony Mannarino
Jacques Beaudry-Losique
Kashif Nawaz
Mingkan Zhang
Ahmed Abuheiba
Praveen Cheekatamarla
Dean Edwards

March 2023

OAK RIDGE National Laboratory

ORNL IS MANAGED BY UT-BATTELLE LLC FOR THE US DEPARTMENT OF ENERGY

ORNL/TM-2023/2883

Building and Transportation Science Division

DEVELOPMENT AND TESTING OF RESIDENTIAL MICRO-CHP POWERED BY OPPOSED PISTON ENGINE

Zhiming Gao [1]
Philip Zoldak [2]
Jonathan Mansinger [2]
Joseph DeMaria [2]
Tony Mannarino [2]
Jacques Beaudry-Losique [2]
Kashif Nawaz [1]
Mingkan Zhang [1]
Ahmed Abuheiba [1]
Cheekatamarla, Praveen [1]
Dean Edwards [1]

March 2023

Prepared by

[1] Oak Ridge National Laboratory
Oak Ridge, TN 37831
managed by
UT-BATTELLE LLC

And

[2] Enginuity Power Systems
730 S Washington St, Alexandria, VA 22314

for the
US DEPARTMENT OF ENERGY
under contract DE-AC05-00OR22725

CONTENTS

LIST OF FIGURES

LIST OF TABLES

ABSTRACT

A micro–combined heat and power (mCHP) prototype powered by innovative inwardly opposed piston engine technology was developed to simultaneously provide electricity and heat to residential or light commercial buildings. The mCHP prototype targeted at residential applications includes an inwardly opposed-piston four-stroke (OP4S) engine, generator, rectifier, inverter, battery energy storage system, 52 gal water tank, and application accessories for hot water supply and space heating. The OP4S engine can The OP4S engine can run on multiple fuels, including renewable gas (biogas), natural gas and propane, as well as hydrogen, to generate mechanical power and waste heat in form of hot coolant and exhaust gas simultaneously. The waste heat is recovered and stored in the water tank and can be used as a regular hot water supply and/or for space heating application. The tests show that the mCHP prototype enabled power outputs in the range of 3.2 –7.4 kW with up to 26.4% of AC electricity efficiency and up to 93.1% of the overall mCHP efficiency under stoichiometric combustion modes $\lambda=\sim1.0$. The mCHP was also run under lean combustion mode conditions at $\lambda=\sim1.3$. The lean mode operation enables more than 30% improvement in electrical energy efficiency. The maximum AC efficiency of the lean combustion mode attained was 35.2%, with the engine efficiency is approaching 40%. The exceptional electrical efficiency breaks the typical upper boundary of 30% for ICE-based mCHP. The engine exhaust temperatures in the lean modes are substantially less than in the stoichiometric modes. Moreover, the lean cases achieve high total mCHP efficiencies: the overall mCHP efficiencies are all greater than 93%. Considering the mCHP prototype can achieve low-cost, flexible matching of thermal and electrical loads while reducing the complexity of distribution and installation, along with high efficiency and fuel flexibility, the novel technology will accelerate the acceptance and adoption of mCHP in the US residential and light commercial markets.

1. INTRODUCTION

1.1 Current mCHP Applications in Buildings

Residential buildings and industrial processes usually require substantial heat and electricity simultaneously. Unfortunately, two-thirds of the energy used by conventional electricity generation is wasted in the form of heat discharged to the atmosphere [1]. Additional energy is further wasted during the distribution of electricity to end users. Combined heat and power (CHP) is a high efficiency energy technology that generates electrical power and captures heat that would otherwise be wasted to provide useful thermal energy —such as steam or hot water used for space heating, hot water supply, and industrial processes —in a single process and from a single energy source [2]. Thus, CHP systems enable more efficient and environmentally friendly energy usage than achieved when heat and electricity are produced in separate processes.

In fact, the exclusive features of CHP contribute to sustainable building solutions, especially the application of micro-combined heat and power (mCHP) systems in single-family houses and multiple-family buildings that demand only a few kilowatts of electricity while requiring substantial space heating and water heating [3]. Thus, mCHP can be used as a decentralized (distributed) system of heat and electricity production and can be installed as independent equipment at an immediate consumption location. Such distributed heat and electricity generation equipment using renewable energy is an excellent solution to reduce greenhouse gas emissions and to increase the grid network security [4,5]. Substantial work has been performed to understand the economic benefit, marketing, and residential applications of mCHP in Asia [6,7,8], Europe [9,10], the Middle East [11], and North America [12]. Jung et.al. [6] reported that the total primary energy consumption, CO_2 emissions and operation cost were reduced by 18.4%, 11.8%, and 9.6%, respectively. However, the payback time is more than 10 years in South Korea because of expensive CHP equipment and facilities. The results stated by Ren and Gao [7] indicated that it was infeasible to introduce the mCHP in China. Giffin's results [12] indicate that the conventional system performs much more efficiently and cost-effective than the CHP system in the United States. However, preliminary deployment of mCHP in Europe seemed practically feasible, especially with operation optimization [9] and appropriate mCHP sizing [10]. Small-scale CHP can be effective in small buildings if the total heat demand is high enough [13]. This result was confirmed by Barbeiri et.al. [14], who showed that mCHP optimization could improve the market penetration in the building sector.

1.2 mCHP Technologies

The major mCHP technologies include internal combustion engines (ICEs), micro gas turbines, micro-Rankine cycles, Stirling engines, and thermophotovoltaic generators [3, 18–24]. Table 1 summarizes these representative technologies available in the public domain. Most commercial mCHPs are powered by ICEs and Stirling engines. Other technologies, such as micro gas turbines, micro-Rankine cycles, and thermo-photovoltaic generators, remain immature and achieve less efficiency compared with ICE and Stirling engine technologies. Unlike ICE, the Stirling engine is an external combustion engine, in which heat is transmitted to the working fluid through an exchanger [25,26]. In a Stirling engine, no direct contact occurs between the combustible gas mixture and all moving mechanical parts, offering better performance at low temperature, greater fuel versatility, and less consequent maintenance. However, Stirling engines are usually larger, heavier, and incur higher capital cost than ICEs. Real Stirling engines usually cannot achieve the efficiencies of ICEs because Stirling engines using regular materials are incapable of supplying heat at 1,500°C–1,600°C by thermal conduction. Therefore, ICE technologies remain the most attractive and well-established technology for the mCHP application, enabling more than 20% electricity efficiency and a

potential mCHP efficiency up to 90% [18,19,21]. Unfortunately, current ICE technologies in mCHP applications do not achieve more than 30% electrical efficiency, as well as enabling low emissions, silent operation, low cost, and reduced maintenance [3]. Continuously developing novel technologies that enhance the efficiency and cost effectiveness of mCHPs is important for extending their market penetration.

Table 1. Summary and characteristics of mCHP for single- family house and small building

Tech.	OEM/academic	Model	Electric power (KW)	Heat power (KW)	Electric efficiency (%)	CHP efficiency (%)	Ref.
ICE (4)	Honda	Ecowill	1	2.8–3	20.0–23.5	74.5–85	[3, 19]
ICE (4)	Senertec	Dachs	5.5	12.5-15.5	24–27.7	61–92	[3,13,21,23]
ICE (4)	Marathon Engine System	Ecopower	1.0–4.7	—	24.4–25	65–84.5	[13,18,23]
Turbine	Academic	Prototype	1.5	4.7	6.3	—	[15]
Turbine	MTT	Prototype	3	15	16	96.0	[3]
Stirling	Solo	Solo 161	2–9.5	8–26	20–26.8	72 –100	[3,13,22,23]
Stirling	Stirling Denmark	SM5A	9	25	19–21	80–88	[23]
Stirling	Whisper Tech	—	0.75-1	4.9–8	6–12	80–82	[13,20]
ORC	Energetix	Genlec	1	8	10	90	[3]
ORC	Academic	Prototype	0.9	47.3	1.41	78.7	[16]
ORC	COGEN Microsystems	Prototype	2.5	11	18.5	99	[3]
TPV	Academic	Prototype	0.3	8.5	1.3–2	83–84	[17]
TPV	JX Crystal	Prototype	1.5	9.4	12.3	92.1	[3]

Note: ICE = internal combustion engine; ORC = organic Rankine cycle; TPV = thermophotovoltaic.

1.3 What Are Opposed- Piston Engines

Opposed- piston engines (OPEs) differ from conventional ICEs wherein the cylinder head is replaced by a second piston so that the two pistons in an OPE move toward each other during compression and away from each other during expansion. The novel architecture doubles the stroke- to- bore ratio. This allows a reduced displacement, but enables a higher power density without excessive piston speed exceeding peak cylinder pressure limits. Compared to a conventional engine, Moreover, OPEs can reduce in-cylinder heat losses because of the elimination of the cylinder head and lower surface area to volume ratio [27]. These features enable a significant gain in thermal efficiency compared with conventional ICEs [28,29]. Additionally, the cost of OPEs is significantly lower than conventional ICEs, mainly because of the lower part count per engine unit. For example, a OPE does not require a head gasket, large multiple head bolts and a cylinder head. Consequently, OPEs are gaining interest in the automotive industry [27, 30–32]. Achates Power Inc. [31, 33] has been developing an opposed-piston two-stroke (OP2S) engine, which shows promise in the automotive industry. Achates claims its OP2S are 30%–50% more efficient than equivalent conventional petrol and diesel engines and 10% cheaper [31]. Enginuity Power Systems (Enginuity) has developed a gaseous fueled boosted opposed-piston four-stroke (OP4S) engine and demonstrated up to 40% energy saving with boosted hydrogen operation [34, 35]. Furthermore, OPEs have been widely considered as a propulsion system in the marine and aviation industries [36-38]. For example, William Doxford and Sons manufactured low-speed marine diesel engines with power up to 20,000 kW [36]. Fairbanks Morse Defense introduced a 3,700 MW OPE marine propulsion system [37]. Gemini Diesel Inc. offered Gemini 100 and Gemini 125 three- cylinder, two-stroke, OPEs for the aviation industry [37]. However, a literature search reveals that no mCHP systems have been powered by an OPE.

1.4 Project Objective

This work reports a novel mCHP prototype powered by a OP4S engine, which is developed by Enginuity in collaboration with the US Department of Energy's Oak Ridge National Laboratory (ORNL), to simultaneously provide heat and electricity to single-family houses or light commercial buildings. The novel mCHP prototype targeted at building applications aims to enable low-cost flexible matching of thermal and electrical loads and to reduce the complexity of distribution and installation while recovering and storing waste heat as hot water. The novel mCHP technology will promote mCHP acceptance in the US residential and light commercial markets, given its low cost and drop-in replacement feature which uses the building's existing connections. This report describes the prototype development of the mCHP system and its performance evaluation over various heat and power outputs.

2. METHODOLOGY AND EXPERIMENTAL SETUP

2.1 mCHP development

The mCHP unit consists of the Enginuity OP4S model V5.1, generator, rectifier, inverter, battery energy storage system, 52 gal water tank, and hot water supply and space heating application. The battery energy storage system is an external accessory component. The unit also includes control modules for engine control using engine control unit (ECU) and mCHP control using programmable logic controller (PLC) to manage engine operation, battery charging, and waste heat recovery. Figures 1(a) and 1(b) shows the entire mCHP unit. In the mCHP, the OP4S can use renewable gas (biogas), natural gas, propane,, as well as hydrogen, to generate mechanical power and waste heat in format of hot coolant and exhaust gas at the same time. The generated mechanical power drives the generator to generate AC electricity, which is used to meet the building's electricity demands or charge the battery after rectification to DC electricity through onboard rectifier or go to the grid. The waste heat in the hot coolant and exhaust flow is recovered and stored in the 52 gal water tank, which is designed to connect to a building's hot water supply and space heating application. Figure 1(c) displays the mCHP system architecture and energy flow.

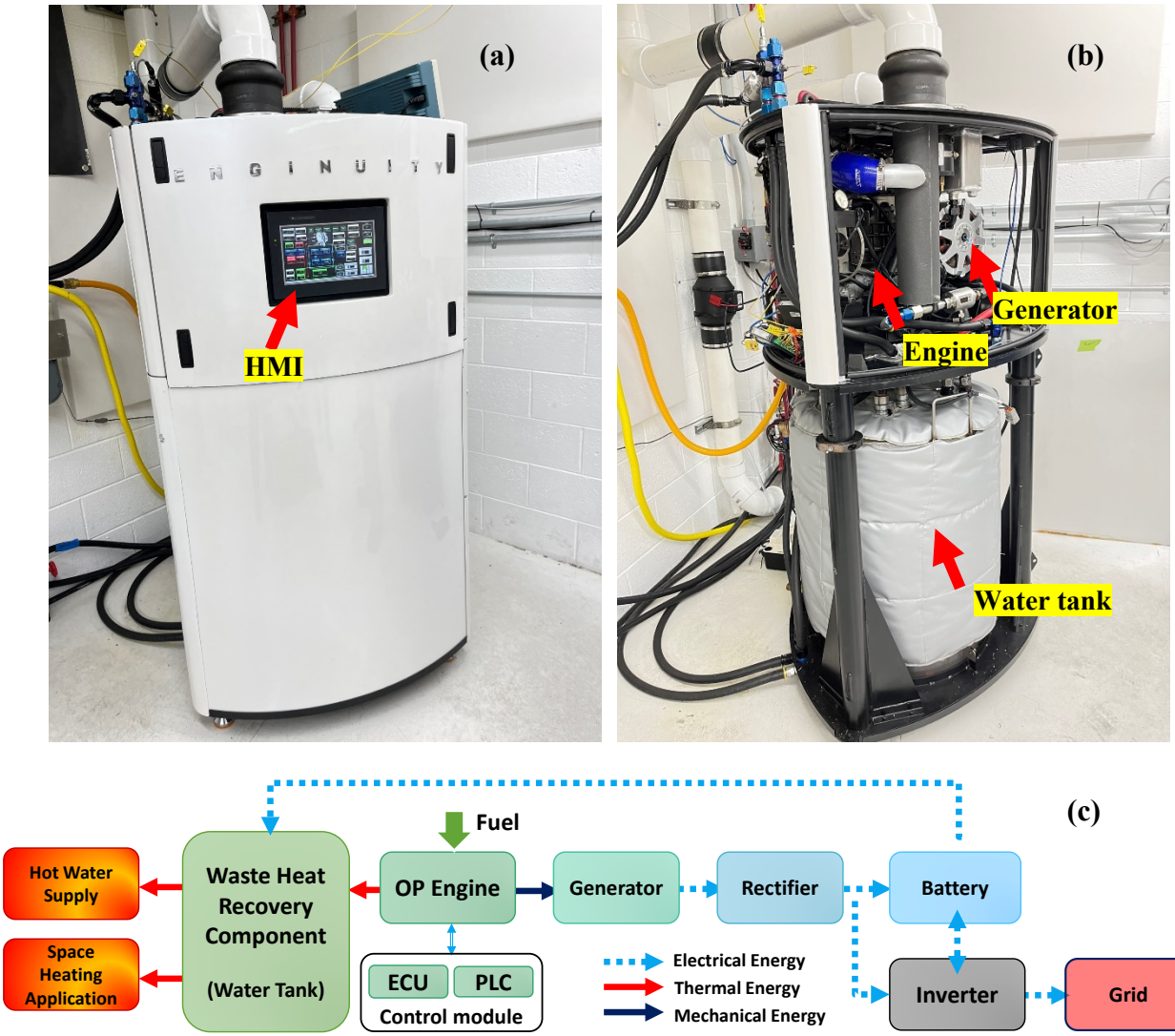

Figure 1. The integrated mCHP system in a testing lab. (a) the external view of mCHP; (b) the internal view of mCHP; (c) mCHP system architecture and energy flow.

The Enginuity OP4S is a single-cylinder spark ignited (SI) engine operating with premixed renewable natural gas or other gaseous fuels containing hydrogen. The configuration and specifications for the engine are shown in Figure 2. In the OP4S, two pistons share one cylinder, each with its own crankshaft and connecting rod. The pistons move toward one another and meet at the top dead center. As the pistons approach each other at the top of each stroke, the premixed natural gas is ignited by spark plug in the cylinder, and combustion occurs, which converts fuel potential energy to work and pushes the pistons apart. The two crankshafts, one on each end of the engine, are joined by a set of gears from which mechanical power is transported to the generator and produces AC electricity. Moreover, in the OP4S, the intake valve and port let the intake air flow into the engine, while the exhaust valve and exhaust port opening lets the exhaust gases flow out of the engine Each piston fires on every second stroke, making this a four-stroke combustion. The ECU and PLC control module shown in Figure 1(c) manages the four-stroke engine operation at either stoichiometric or lean combustion mode. Unlike conventional ICEs which route the substantial heat of combustion to the cylinder head, the heat of combustion in the OP4S goes to the opposing piston only, enabling- less heat loss and higher efficiency.

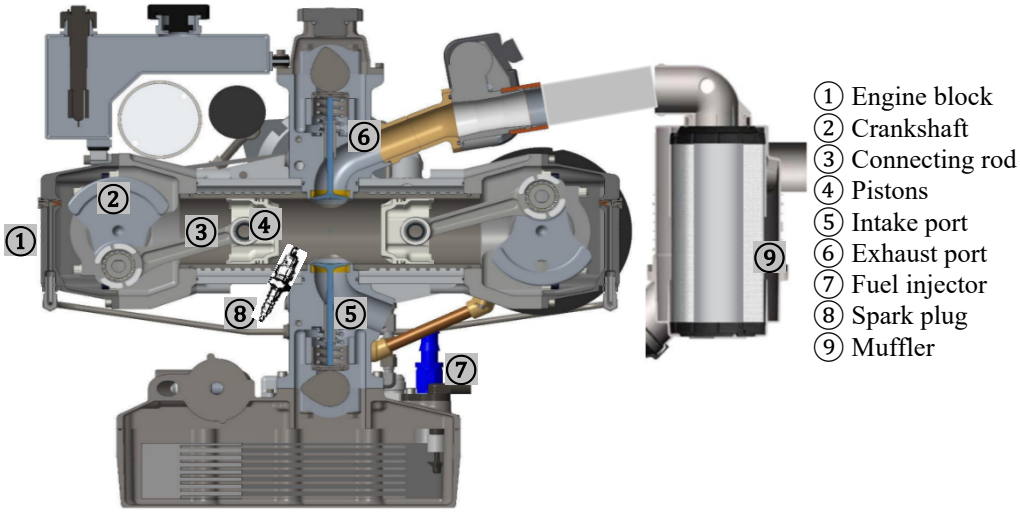

Bore	67 mm
Half- stroke	71 mm
Bore/half- stroke ratio	0.944
Connecting rod length	125.30 mm
Half- cylinder displacement	250.3 cm^3
Connecting rod length/stroke ratio	1.765
Crank radius	35.5 mm
Compression ratio	8.5

Figure 2. (a) Configuration of Enginuity OP4S and (b) the specifications of Enginuity OP4S

In the mCHP, waste heat from the OP4S is recovered in two ways: by using coolant flow circuit and by using the exhaust gas coil. To enable efficient engine operation and proper lubrication, the proposed mCHP includes a thermostat to maintain the returning coolant temperature around 70–80°C to the engine based on splitting the coolant flow come from the engine into two separated streams: (1) partial coolant flow enters the waste heat recovery component, and (2) major coolant flow bypasses the waste heat recovery component to mix with the cooled coolant from the waste heat recovery component. The recovered thermal

energy is stored in the water tank and can be used as a domestic hot water supply as well as for potential space heating applications. Figure 3 shows the configuration of this mCHP waste heat recovery component, which includes a large-diameter helical coil for exhaust heat recovery and a small-diameter helical inner coil for waste heat recovery of the coolant. The water tank is designed to connect with two different electric heating elements, AC and DC electric heating, with two different power ratings. When the engine is off, the water tank can be heated by these electric heaters from the battery energy storage system or the external grid. The design allows the system to operate more efficiently while meeting the flexible heat demands. This approach also lowers emission significantly in a cost-effective manner.

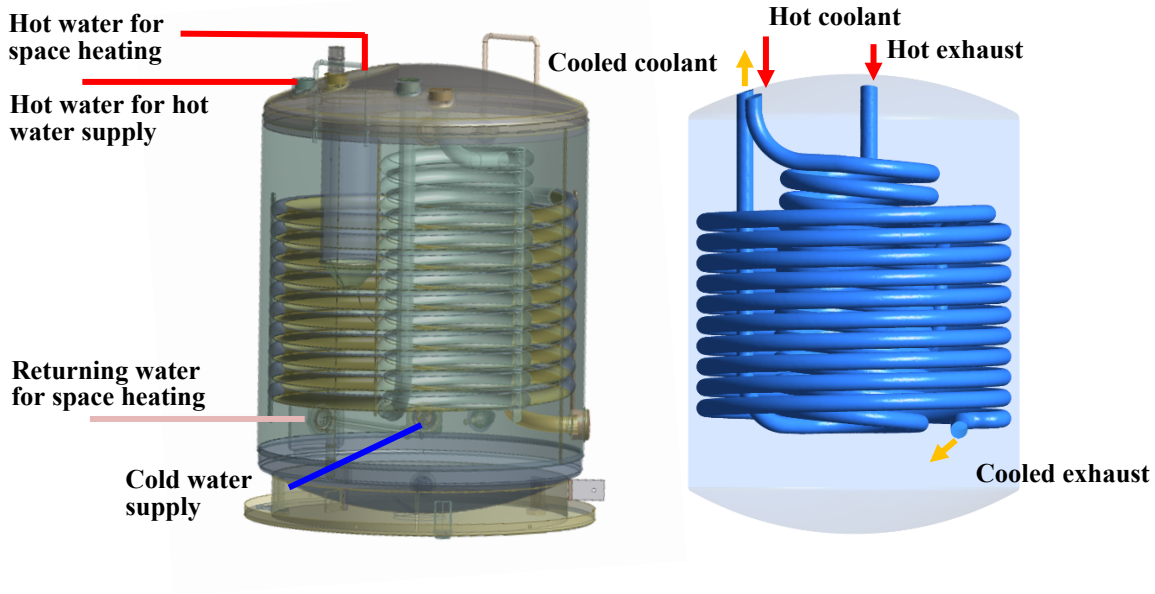

Figure 3. (a) Configuration of mCHP waste heat recovery component and (b) the simplified architecture of mCHP waste heat recovery component showing the helical coils for exhaust and coolant waste heat recovery.

2.2 mCHP Experimental Setup

The developed mCHP was installed and tested Test Cell 7 at Enginuity's testing facility, located in Clinton Township, MI location, shown in Figure 4 in the supplemental document. Because the testing facility and real residential homes have different infrastructure for hot water supply and space heating applications, the thermal load was alternatively imposed by adding an intermediate compact plate heat exchanger to transfer heat from hot water from the mCHP's water tank to the cooling loop in the testing facility. The cooled supply water was then returned to the water tank instead of to the real direct hot water supply. The space heating application was designed to directly deliver hot water from the mCHP's water tank to a space heating device.

Figure 4: Enginuity's mCHP testing facility enabling electrical battery charging, water and space heating

To collect the data for comprehensively analyzing the mCHP system, the thermocouples and flow meters for air, fuel, and coolant flows, as well as the sensors for electricity current and voltage measurement, are appropriately installed in the system, as shown in Figure 5. The table listed in Figure 5 further explains the detailed measurement parameters for flows, temperatures, and electricity. The key measurements include fuel consumption, battery current and voltage, lambda sensor or O_2 sensor, exhaust temperature at the inlet and outlet of water tank, coolant temperature at the inlet and outlet of water tank, coolant flow, water flow and inlet and outlet temperature for household hot water supply, and water flow and inlet and outlet temperature for space heating. The data from these sensors are collected by the PLC modules, which, along with the ECU, control the mCHP systems.

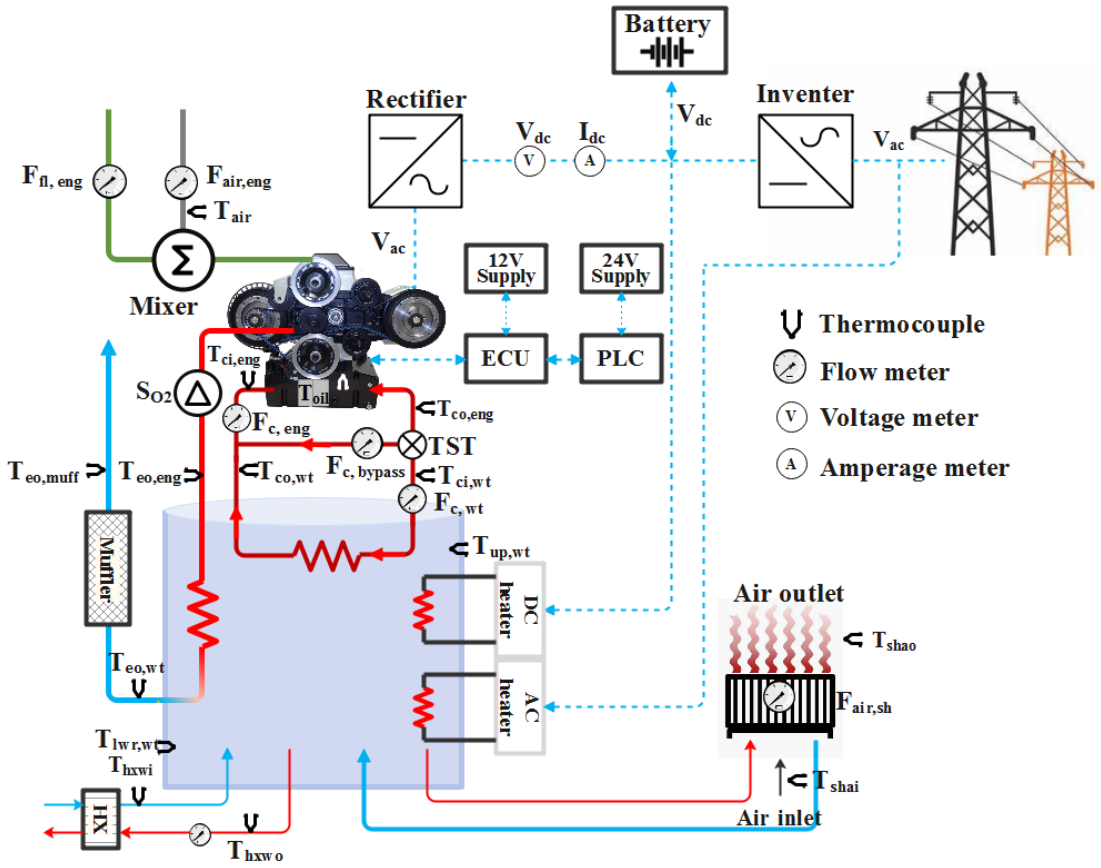

Label	Description	Label	Description
$T_{eo,eng}$	Thermocouple for exhaust @ engine out	$F_{fl,eng}$	Natural gas flow for engine
$T_{eo,wt}$	Thermocouple for exhaust @ water tank out	$F_{air,eng}$	Air flow for engine
$T_{eo,muff}$	Thermocouple for exhaust @ muffler out	$F_{c,eng}$	Coolant flow for engine
$T_{co,eng}$	Thermocouple for coolant @ engine out	$F_{c,wt}$	Coolant Flow for water tank
$T_{ci,eng}$	Thermocouple for coolant @ engine in	$F_{c,pass}$	Coolant Flow for bypass loop
T_{oil}	Thermocouple for engine oil	$F_{air,sh}$	Air flow for space heating
T_{air}	Thermocouple for engine air in	F_{hxwf}	Heat exchanger water flow
$T_{ci,wt}$	Thermocouple for coolant @ water tank in	S_{O2}	Oxygen sensor
$T_{co,wt}$	Thermocouple for coolant @ water tank out	TST	Thermostat mechanical flow valve
$T_{up,wt}$	Thermocouple for water @ upper tank	V_{ac}	AC voltage
$T_{lwr,wt}$	Thermocouple for water @ lower tank	V_{dc}	DC voltage
T_{hxwi}	Thermocouple for water @heat exchanger in	I_{dc}	DC current
T_{hxwo}	Thermocouple for water @ heat exchanger out	ECU	Engine Control Unit
T_{shai}	Thermocouple at space heating air in	PLC	Programmable Logic Control
T_{shao}	Thermocouple at space heating air out	Mixer	Air and fuel mixer

Figure 5. Schematic of the mCHP testing system and sensor map; ▪▪▪▪ represents electrical energy; ▬ represents hot thermal energy; ▬ represents cold thermal energy; ▬ represents fuel energy.

2.3 Efficiency Analysis Methodology

In the study, the electric efficiency η_e is defined by the first law of thermodynamics as electrical energy flow $\dot{w}_e$ divided by fuel energy consumption rate $\dot{Q}_{f,LHV}$ based on fuel low heating value (LHV). The electrical energy $\dot{w}_e$ considered here could be AC electricity after generator or DC electricity before charging the battery. The AC electric efficiency $\eta_{e,ac}$ and DC electric efficiency $\eta_{e,dc}$ can also be descried as a function of engine efficiency, generator efficiency, and rectifier efficiency, given by Eqs. (1) and (2).

$$\eta_{e,ac} = \frac{\dot{w}_{e,AC}}{\dot{Q}_{f,LHV}} = \eta_{eng} \cdot \eta_{gen} \#(1)$$

$$\eta_{e,dc} = \frac{\dot{w}_{e,DC}}{\dot{Q}_{f,LHV}} = \eta_{eng} \cdot \eta_{gen} \cdot \eta_{rect} \#(2)$$

A mCHP typically produces useful thermal energy in addition to electricity. Consequently, the overall mCHP efficiency η_{chp} is addressed by adding the useful thermal energy flow $\dot{Q}_{th}$ to the electrical energy rate w_e and divided by fuel energy consumption flow $\dot{Q}_{f,HHV}$ based on fuel higher heating value (HHV). In the current CHP configuration, η_{chp} is shown as below based on DC electrical energy rate.

$$\eta_{chp} = \frac{\dot{w}_{e,dc} + \sum \dot{Q}_{th}}{\dot{Q}_{f,HHV}} \#(3)$$

In these equations, the fuel energy consumption flows, $\dot{Q}_{f,HHV}$ and $\dot{Q}_{f.LHV}$, are calculated based on fuel mass flow multiplied with fuel higher heating value and LHV, respectively. The higher heating value (also known gross calorific value) of a fuel is defined as the amount of heat released by a specified quantity (initially at 25°C) once it is combusted and the products have returned to a temperature of 25°C, which considers the latent heat of vaporization of water in the combustion products. The lower heating value (also known as net calorific value) of a fuel is defined as the amount of heat released by combusting a specified quantity (initially at 25°C) and returning the temperature of the combustion products to 150°C, in which the latent heat of vaporization of water in the reaction products is not recovered.

3. mCHP OPERATION WITH STOICHIOMETRIC MODE

The Enginuity designed mCHP prototype enables flexible electricity outputs to meet dynamic electricity and thermal energy demands for single-family houses or multiple-family buildings. The unit can provide up to 12 kW of electrical power. However, the control module limits its maximum power at 8.0 kW by considering the safety, reliability, and durability of the prototype OP4S, which is still under development. To evaluate, six scenarios were tested. These scenarios are listed in Table 2. All the cases operated at stoichiometric combustion modes with the air fuel ratio set to $\lambda=\sim1.0$. The first three scenarios measured the electric efficiency and overall mCHP thermal efficiency with waste heat recovered and stored in the water tank at various electric power generation. The fourth, fifth and sixth scenarios measured the electric efficiency and overall mCHP thermal efficiency with external thermal demand hot water supply and space heating at different electric power generation.

Table 2. Six testing scenarios for evaluating the mCHP performance at the stoichiometric modes.

Scenario	Description
1	3.5 kW electricity with waste heat recovered and stored in the water tank; the water tank is heated from 26.7 °C to 60 °C without external heat demand.
2	4.5 kW electricity with waste heat recovered and stored in the water tank; the water tank is heated from 26.7 °C to 60 °C without external heat demand.
3	7.5 kW electricity with waste heat recovered and stored in the water tank; the water tank is heated from 61.1 °C to 71.1 °C without external heat demand.
4	3.5 kW electricity with external thermal demand for hot water supply and space heating; the water tank temperature starts at 40 °C
5	4.5 kW electricity with external thermal demand for hot water supply and space heating; the water tank temperature starts at 40 °C
6	6.0 kW electricity with external thermal demand for hot water supply and space heating; the water tank temperature starts at 40 °C

3.1 Electric Efficiency under Stoichiometric Modes

Table 3 shows the electrical power output of the mCHP with the peak AC electricity efficiency of 26.4%. The power outputs are in the range of 3.2 –7.4 kW for the selected six scenarios. Their AC electricity efficiencies vary between 16.8% and 26.4%, and the DC electricity efficiencies vary between 16.1% and 25.3%. The results reveal that larger electric power output leads to higher electric efficiency, whether waste heat is recovered and stored in the water tank or external thermal load is applied for hot water supply and space heating. This expected result occurs because engine throttling loss usually decreases with higher engine power. Figure 6 details the energy flow and efficiencies for each mCHP component and system for the waste heat recovery scenario. Figure 7 details the energy flow and efficiencies for each mCHP component and system for the hot water supply and space heating scenario. The details on energy flow are discussed in the 3.1.2 section.

Table 3. Electric efficiency of the mCHP prototype operating at the stoichiometric modes.

Parameter \ **Scenario**	Waste heat recovered and stored in the tank			Thermal load for hot water supply and space heating		
	1	**2**	**3**	**4**	**5**	**6**
Engine speed (rpm)	2,877	2,900	3,050	2,776	2,918	2,883
Electrical power (kW)	3.7	4.4	7.4	3.2	4.5	5.9
Engine brake energy efficiency (%)	19.1	20.5	29.2	18.6	20.5	28.4
DC electrical power efficiency (%)	16.5	17.2	25.3	16.1	17.7	24.5
AC electrical power efficiency (%)	17.2	17.9	26.4	16.8	18.4	25.5

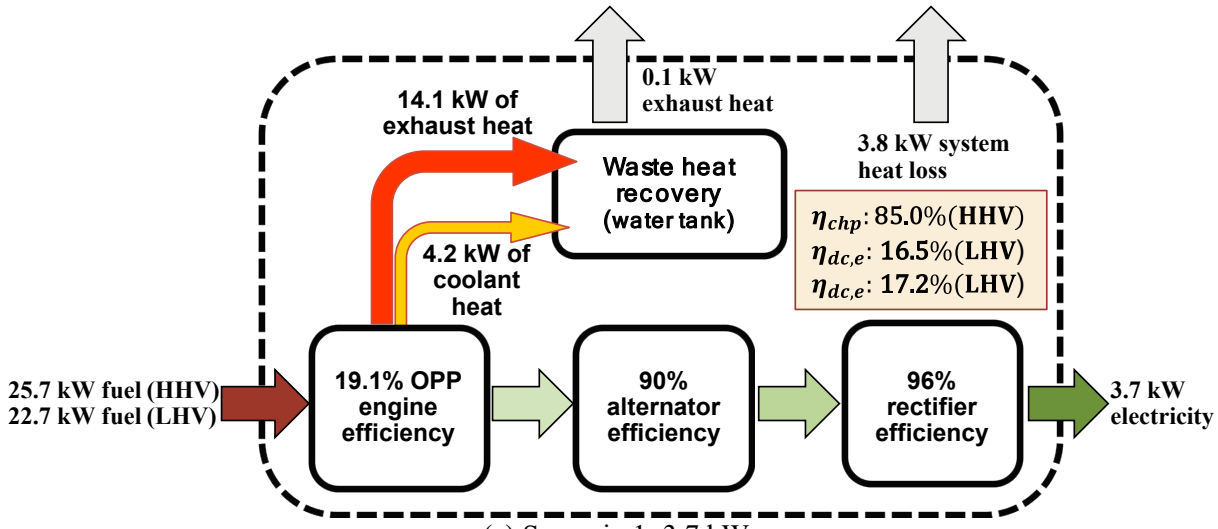

(a) Scenario 1: 3.7 kW

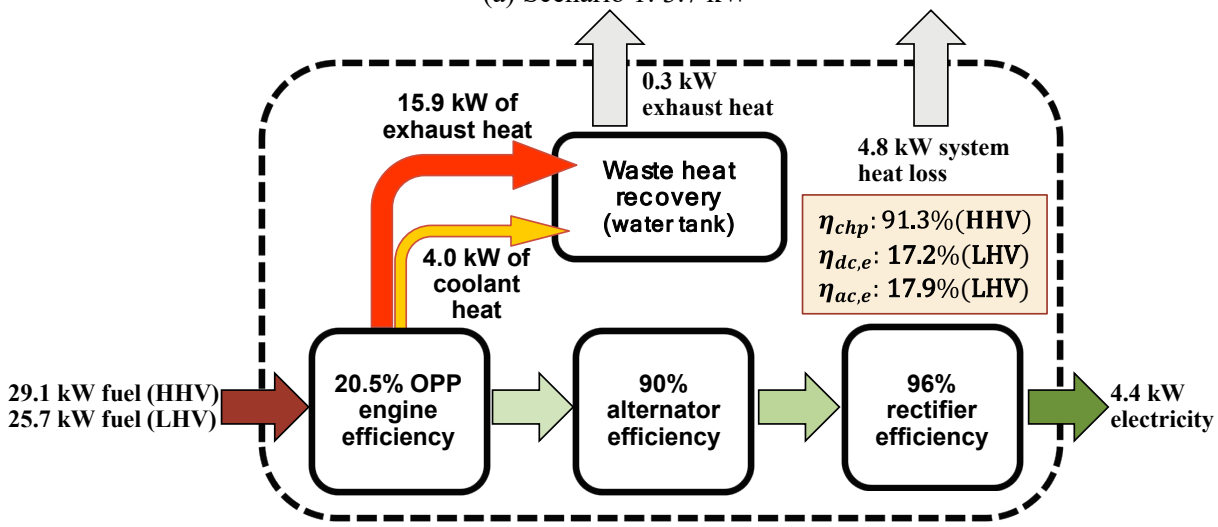

(b) Scenario 2: 4.4 kW

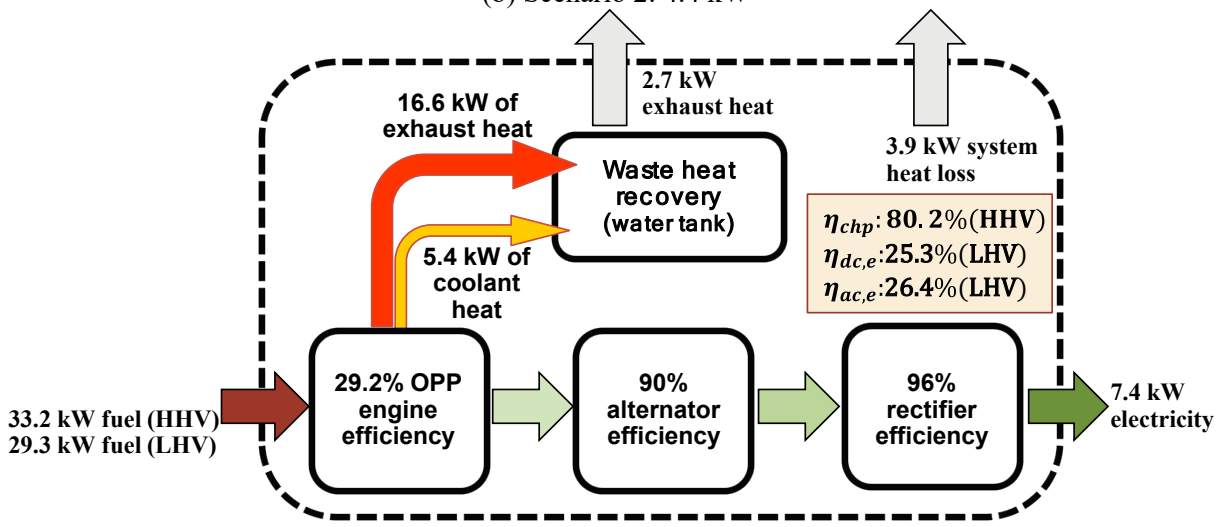

(c) Scenario 3: 7.4 kW

Figure 6. Energy flow and efficiencies for mCHP component and system with waste heat recovered and stored in the water tank. The mCHP operated at stoichiometric modes.

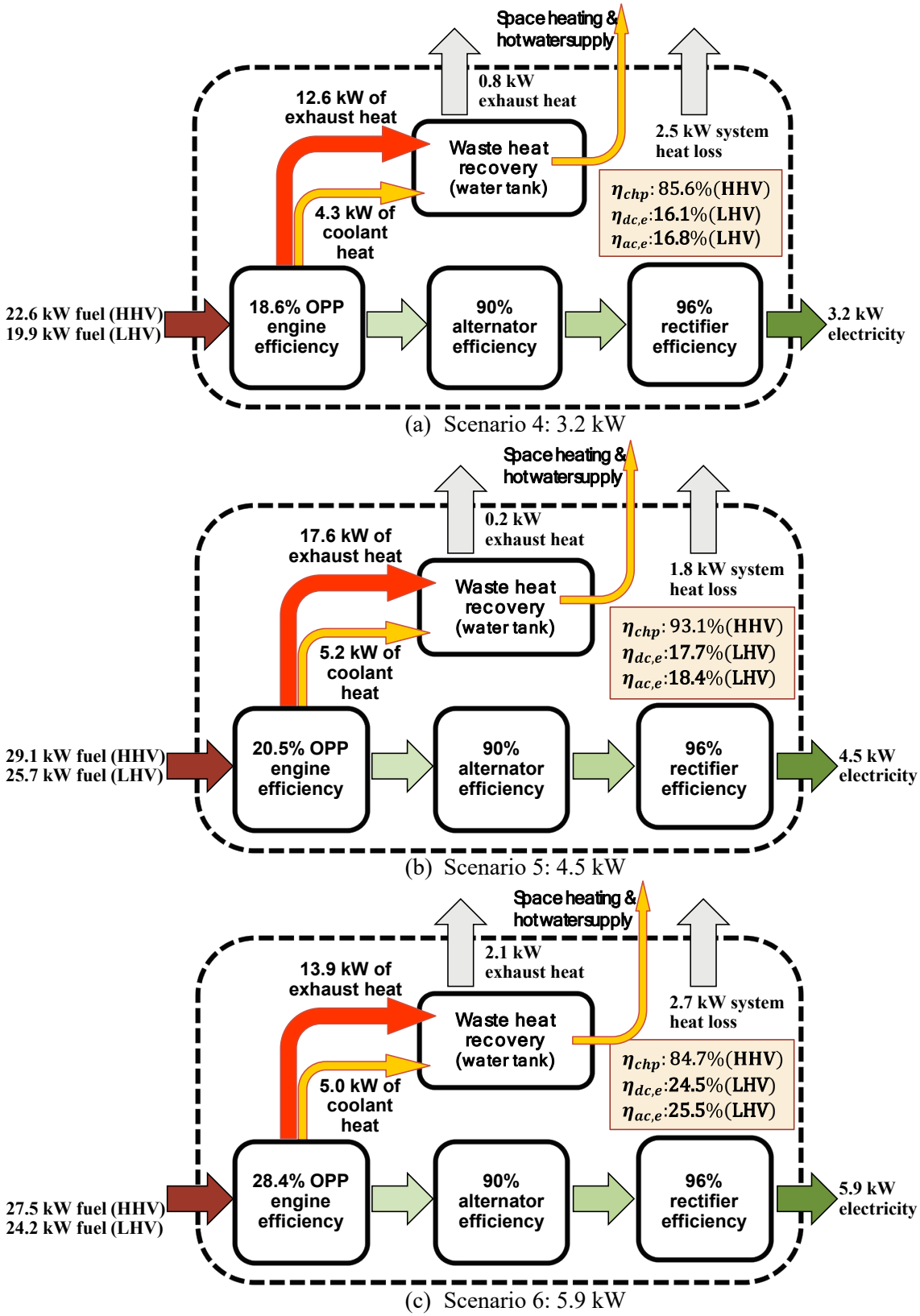

Figure 7. Energy flow and efficiencies for mCHP component and system with external thermal load for hot water supply and space heating. The mCHP operated at stoichiometric modes.

Figure 8 shows the steady-state electric efficiency and 7.4 kW power generated by the mCHP. In the mCHP, the efficiencies of the alternator and rectifier are around 90% and 96%, respectively. These values indicate that the fuel-to-torque efficiency of the OPE is 29.2% in the case of 7.4 kW power generated by the unit. The typical fuel-to-torque efficiency of the commercial four-stroke port fuel-injected and direct gasoline injection engines is around 17% and 22%, respectively, at 7.4 kW [39, 40, 41]. The Enginuity OP4S achieves higher efficiency than conventional commercially available port-fueled-injected SI gasoline engines. A comparable natural gas engine's efficiency is typically less than that of a gasoline engine because gasoline is a liquid fuel, enabling a better volumetric efficiency than a gaseous fueled engine. Thus, to better evaluate the OP4S performance, it can be compared with a commercially available natural gas engine. Figure 9 compares engine brake energy efficiency between the OPE and Cummins Westport natural gas engine as a function of engine power output. Clearly, the OP4S achieves better efficiency at the same given power output.

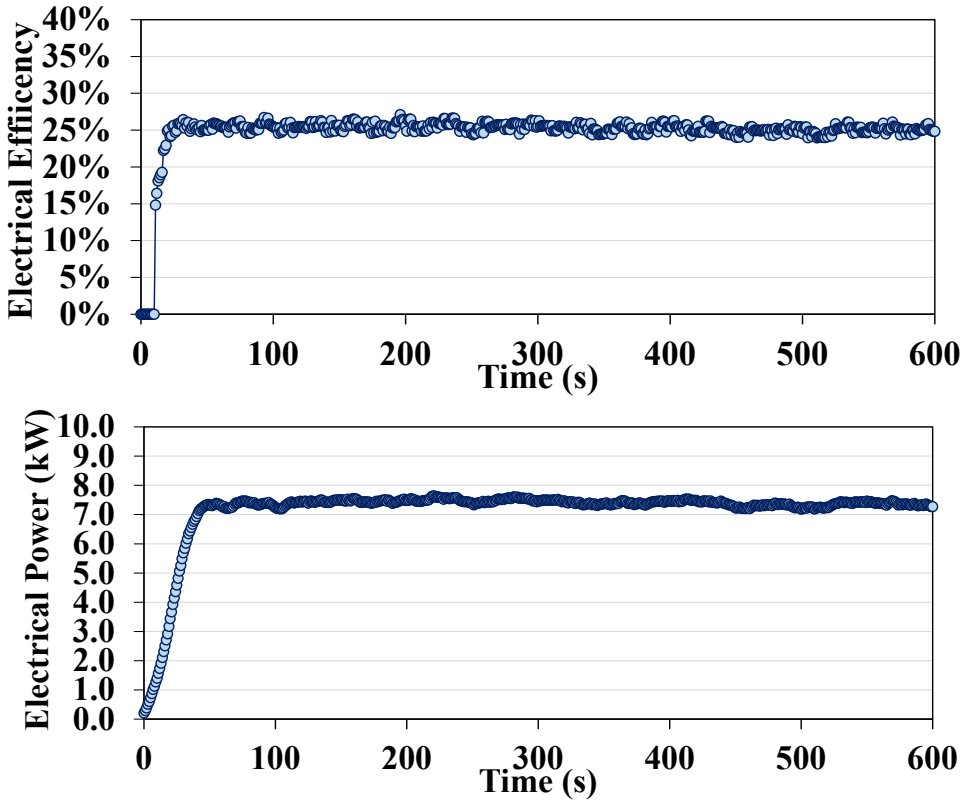

Figure 8. Electric efficiency and power generation of 7.4 kW by the mCHP using the OP4S. Engine speed is 3,050 rpm in the stoichiometric mode.

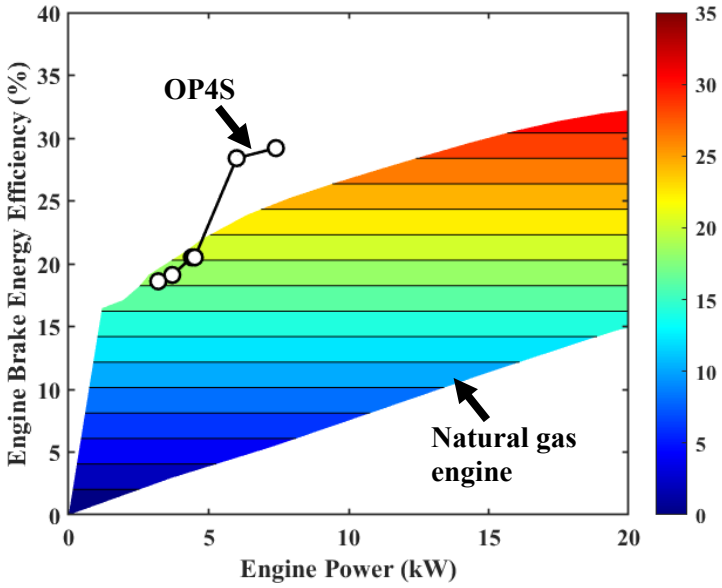

Figure 9. Comparison of engine brake energy efficiency for the OP4S and commercial natural gas engine as a function engine power output (<20 kW). Both engines were operated in the stoichiometric mode. The color bar shows the natural gas engine brake energy efficiency.

The current commercial mCHP products, which are typically powered by ICEs provide 25% electrical efficiency for the electric power of no more than 8.0 kW (see Table 1), the peak AC electricity efficiency of 26.4% is comparable to or better than the commercial products and other prototypes available in the market. Considering that the OP4S currently used in the mCHP adopts stoichiometric combustion, the OP4S and mCHP have great potential to further improve engine efficiency and electricity efficiencies by means of lean combustion technology. Preliminary tests show that the lean combustion model can achieve more than 22% better engine efficiency than the stoichiometric combustion mode in the OP4S. More results are provided in the "lean combustion cases" section.

3.2 Thermal Energy Performance at the Stoichiometric Modes

One of the key advantages to the mCHP application in the building sector is it can provide flexible and useful heat for single-family houses or multiple-family buildings. Based on Figures 6 and 7, the mCHP has 1.8–4.8 kW of system heat loss depending on the cases, while exhaust heat released to ambient conditions is around 0.1–2.7 kW. Such system heat loss is 6.2% –16.5% of HHV fuel energy, and exhaust heat released to ambient condition is around 0.4%–8.1% of HHV fuel energy. Thus, the mCHP system designed is very efficient. Table 4 lists the thermal energy performance of the mCHP prototype for the six scenarios tested. The results demonstrate that the overall mCHP efficiency is up to 93.1%, and the overall mCHP efficiency in all the cases is above 80%.

Table 4. Thermal energy performance of the mCHP prototype at the stoichiometric modes

Parameter \ Scenario	Waste heat recovered and stored in the tank			Thermal load for hot water supply and space heating		
	1	**2**	**3**	**4**	**5**	**6**
Exhaust temperature at entrance of water tank (°C)	823.6	822.6	777.0	813.0	820.0	764.0
Exhaust temperature at exist of water tank (°C)	31.3	38.0	149.9	77.8	36.6	138.3
Coolant temperature an entrance of engine (°C)	77.7	79.3	84.7	79.7	78.2	78.7
Coolant temperature an exist of engine (°C)	73.7	73.1	79.1	73.7	71.5	72.7
Exhaust waste recovery (kW)	14.0	15.6	13.8	11.8	17.4	11.8
Coolant waste recovery (kW)	4.2	4.0	5.4	4.3	5.2	5.0
Overall mCHP efficiency (%)	85.0	91.3	80.2	85.6	93.1	84.7

The observations from Table 4 reveal that most of the waste heat recovery from the developed mCHP in the stoichiometric modes is contributed by hot exhaust from the OP4S. This is mainly because engine exhaust temperature is 700°C–800°C compared with 70°C–85 °C of coolant temperature. In the mCHP, exhaust temperature could be cooled to 31.3 °C to maximize thermal energy use from the fuel. Instead, when exhaust temperature is not cooled sufficiently, the overall mCHP efficiency is degraded. For example, in scenarios 3 and 6, exhaust temperature at the exit of the water tank is 149.9° C and 138.3° C, respectively, resulting in overall mCHP efficiencies of 80.2% and 84.7%, respectively, which are substantially less than the other scenarios. However, because the exhaust temperature is 700°C–800°C, significant opportunity and potential exists for the OP4S via lean combustion to improve the efficiency in the future. Unlike exhaust temperature, to ensure engine operation efficiency and lubricant performance, the coolant temperature was managed around 70°C–80°C by the control module in the mCHP, ensuring a coolant temperature difference of no more than 8 K.

Figure 10 shows an example of the mCHP prototype under the testing conditions of scenario 1 (i.e., 3.7 kW), in which waste heat was recovered and stored in the water tank. In this case, the water tank was heated from 26.7°C to 60°C. The water temperature at the upper location was heated, but the bottom location remained at 26.6°C. Significant temperature stratification occurred in the water tank. This result was confirmed by performing high-fidelity computational fluid dynamics simulations via ANSYS Fluent commercial software. The simulation results for the waste heat recovery component are shown in Figure 11. The result shows the water tank's status at 960 s. Figure 12 shows an example of the mCHP prototype under the testing conditions of scenario 5 (i.e., 4.4 kW), which has external thermal load for hot water supply and space heating. In this case, the recovered heat was continuously used for space heating and hot water supply while the water temperature was maintained at 40° C. The air temperature increased from 26.4°C to 37.7°C; the hot water supply temperature was 38.8°C, and the returning temperature was 27.7° C.

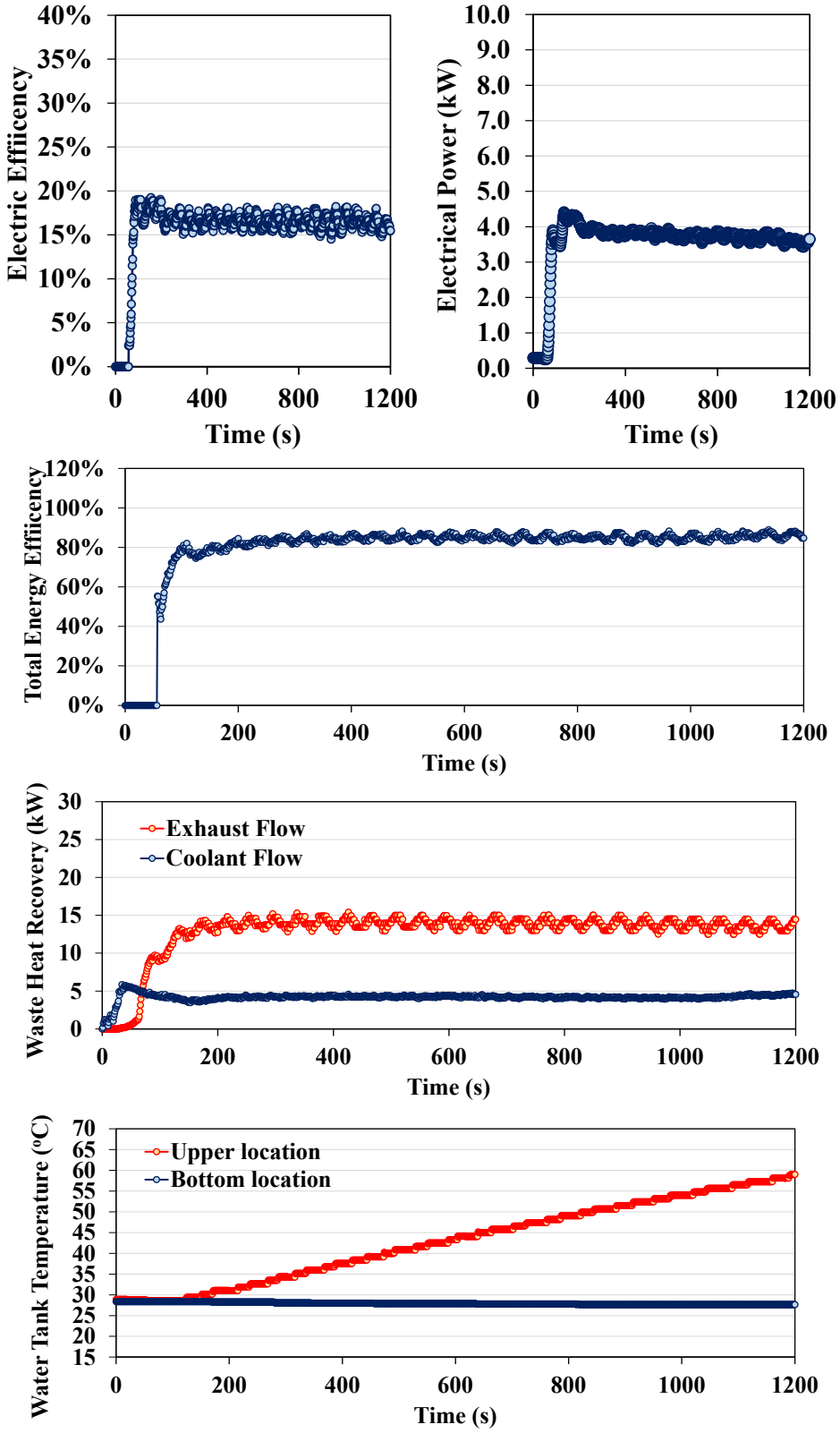

Figure 10. The mCHP prototype performance under the testing conditions of 3.7 kW and with waste heat recovered and stored in the water tank.

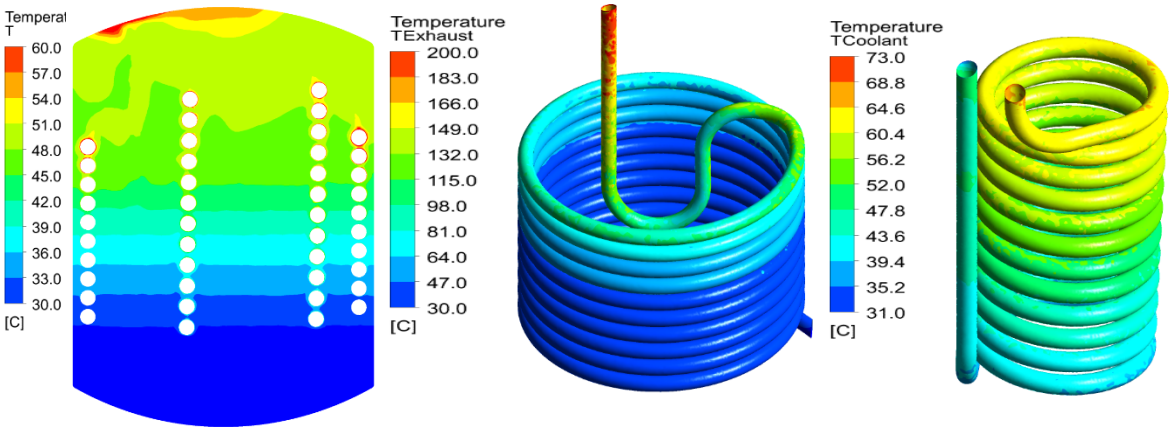

Figure 11. High-fidelity computational fluid dynamics simulation on the mCHP waste heat recovery component.

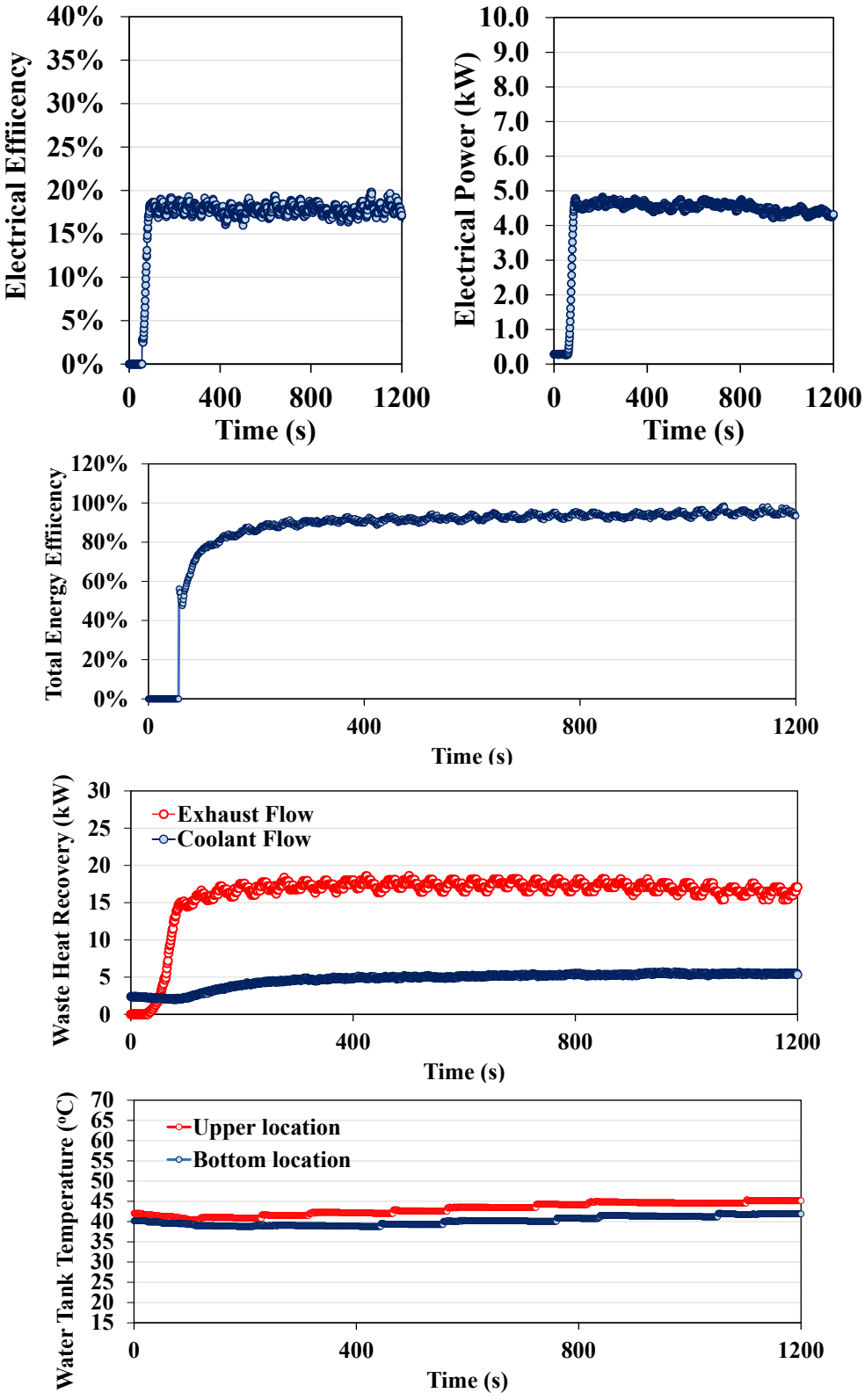

Figure 12. The mCHP prototype performance under the testing conditions of 4.4 kW and with external thermal load for hot water supply and space heating.

4. mCHP OPERATION WITH LEAN COMBUSTION MODE

The effect of lean combustion modes on the OP4S and mCHP performance was explored. Four cases were tested, shown in Tables 5 and 6. The fourth case aims to repeat the third case. All the lean cases enable waste heat recovered and stored in the tank. In all the cases, the control module used the lambda sensor and intake port actuator to maintain a 30% excess of air consumption or λ=~1.3, and also the ignition timing for all lean modes was advanced approximately 10 CAD in order to maximize torque operation compared to the stoichiometric modes. Figure 13 compares the engine and AC electrical efficiencies of the lean and stoichiometric modes. The results indicate that the lean modes achieve more than 35% energy efficiency improvement. The maximum AC electrical efficiency of the lean combustion achieves 35.2%, as the engine efficiency approaches 40%. The electrical efficiency breaks the upper boundary of 30% for ICE-based mCHP. The result further confirmed that the engine exhaust temperatures in the lean modes are substantially less than in the stoichiometric modes, shown in Figure 13. Furthermore, the lean combustion cases achieve higher mCHP efficiencies, shown in Figure 14. All the overall mCHP efficiencies are greater than 93%. The phenomenon may be due to less energy loss in the lean combustion modes. Since engine out exhaust temperatures are lower and the heat exchanger out temperatures are lower, this means that less exhaust heat is lost and more is extracted by the heat exchanger on a percentage basis of total versus the stoichiometric modes. Additionally, since exhaust temp at exhaust valve closing is lower than for stoichiometric mode, the energy released during combustion goes into doing useful mechanical work rather than into exhaust heat which cannot be as effectively transferred via the heat exchanger. This results in and overall improvement of the mCHP efficiency.

Table 5. Electric efficiency performance of the mCHP prototype in lean combustion mode

Parameter \ Scenario	Waste heat recovered and stored in the tank			
	1	**2**	**3**	**4***
Engine speed (RPM)	2,705	2,780	2,850	2904
Electrical power (kW)	3.5	4.4	5.7	5.8
Engine brake energy efficiency (%)	25.2	32.4	39.1	38.7
AC electrical power efficiency (%)	22.7	29.2	35.2	34.8
DC electrical power efficiency (%)	21.8	28.0	33.8	33.4

Table 6. Thermal energy performance of the mCHP prototype in lean combustion mode

Parameter \ Scenario	Waste heat recovered and stored in the tank			
	1	**2**	**3**	**4***
Exhaust temperature at entrance of water tank (°C)	747.6	698	692	699
Exhaust temperature at exist of water tank (°C)	46.7	44.6	47.7	43.4
Coolant temperature at entrance of engine (°C)	74.1	74.3	74.5	73.8
Coolant temperature at exist of engine (°C)	79.1	79.2	79.0	79.4
Exhaust waste recovery (kW)	9.4	9.1	9.4	9.9
Coolant waste recovery (kW)	4.2	3.2	2.8	2.5
Overall CHP efficiency (%)	94.0	93.1	93.3	93.7

** The case 4 aims to repeat the case 3.*

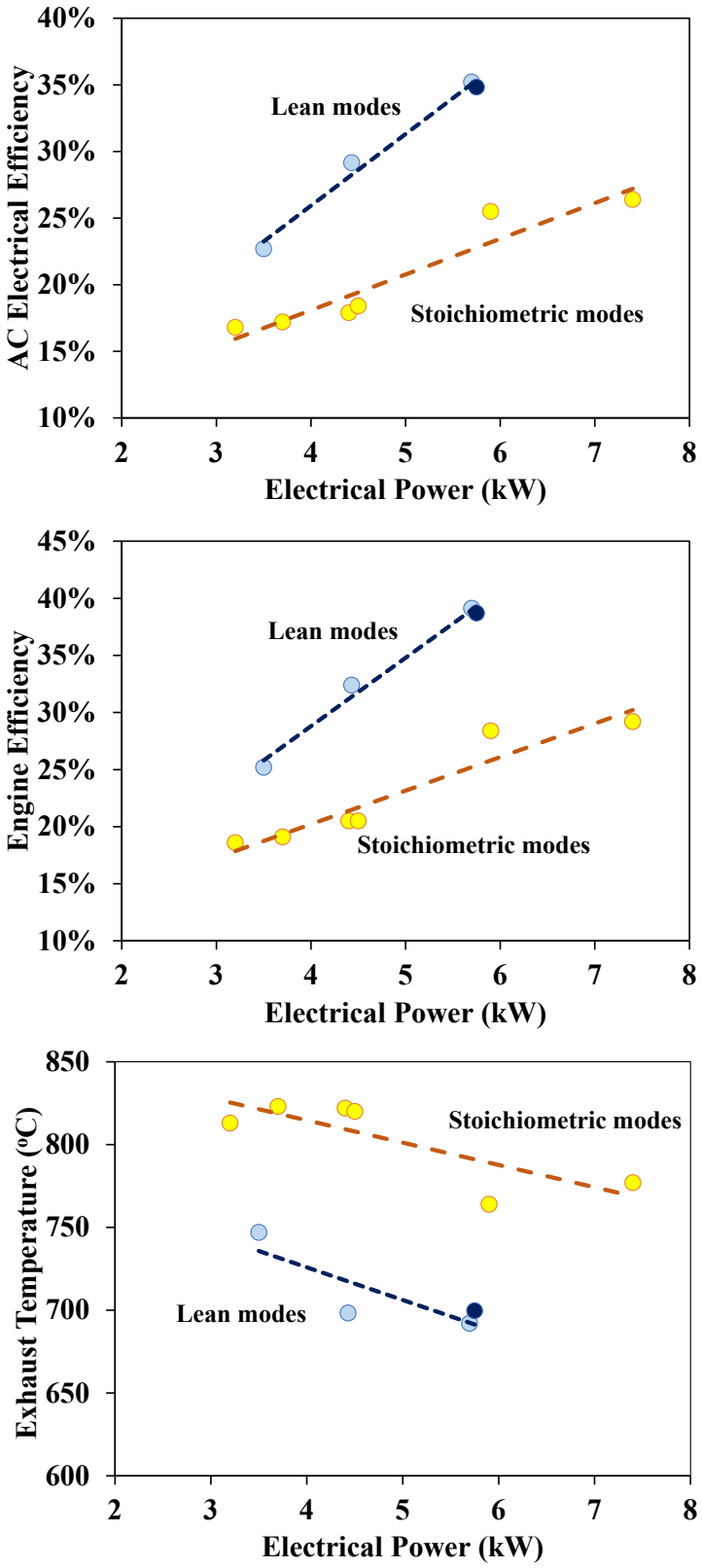

Figure 13. Comparison of engine and AC electrical efficiencies between lean and stoichiometric modes.

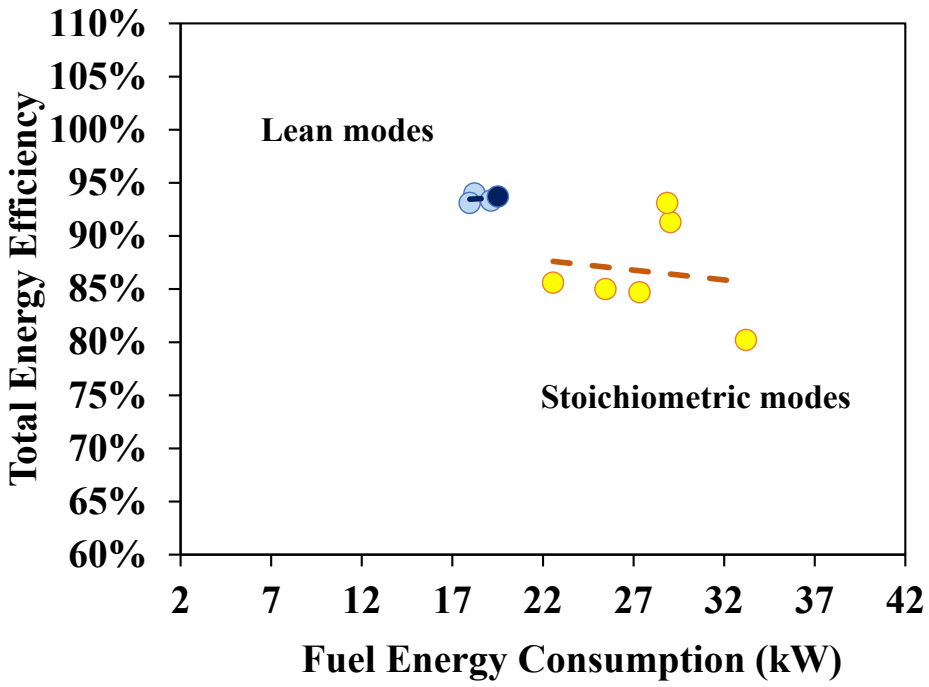

Figure 14. Comparison of the overall mCHP efficiencies between lean and stoichiometric modes.

Figure 15 shows the mCHP prototype performance under the testing conditions of 5.7 kW at lean combustion mode and with waste heat recovered and stored in the water tank. Figure 16 shows energy flow and efficiencies for mCHP component and system operated at lean combustion mode. The lean combustion mode is expected to achieve even higher electrical efficiency in the proposed mCHP for the cases of 6.0 kW or higher. However, hardware limitations precluded running the cases of more than 6.0 kW at lean combustion modes. This is because the maximum air flow of the engine is limited with wide open throttle (WOT) operation. In the studied lean combustion modes, to run lean burn with 30% excessive air, the fuel delivery has to trim the amount of fuel being injected by 30% which limits the amount of mechanical power the engine is able to produce at the brake at rated power conditions.

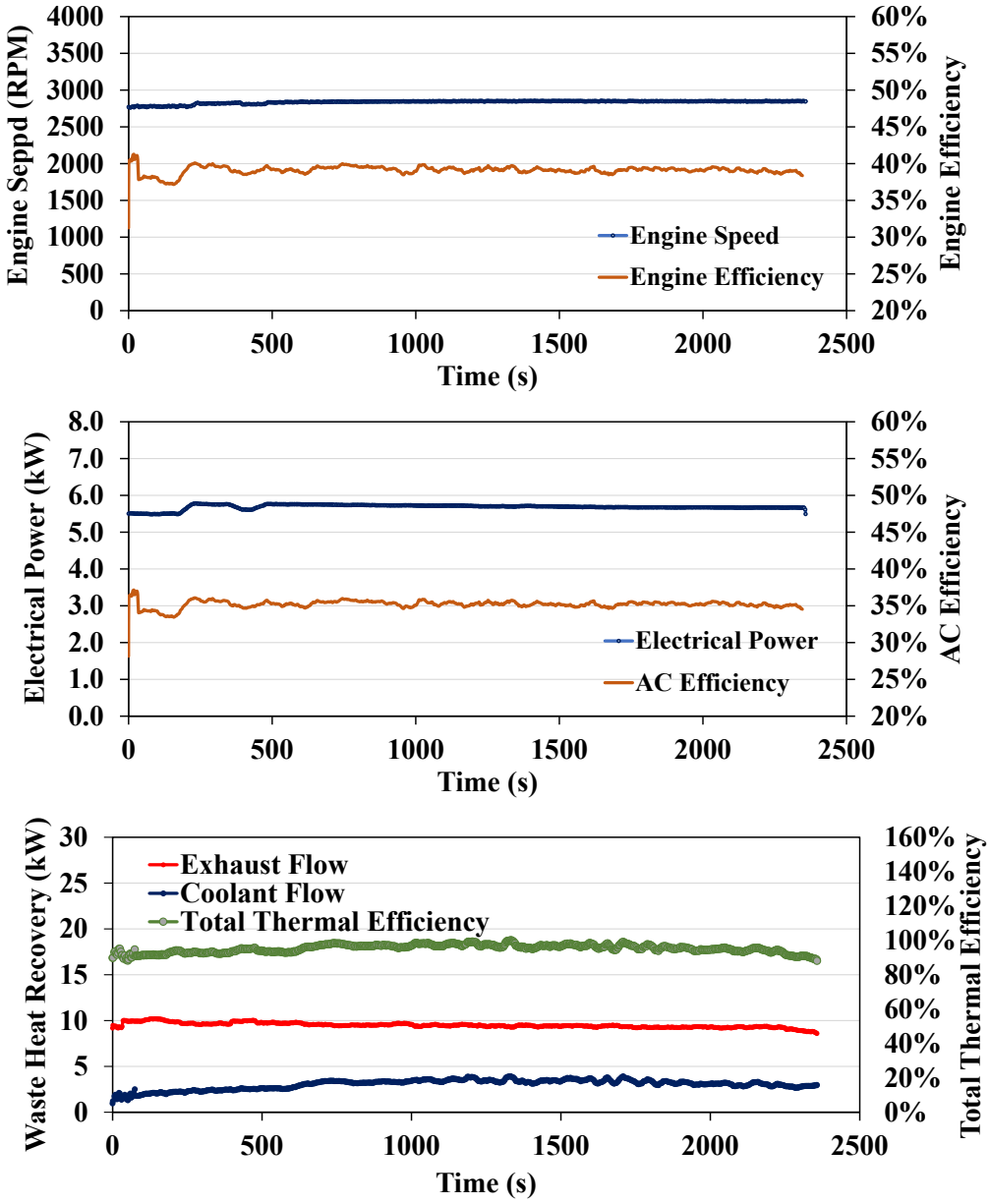

Figure 15. The mCHP prototype performance under the testing conditions of 5.7 kW at lean combustion mode and with waste heat recovered and stored in the water tank.

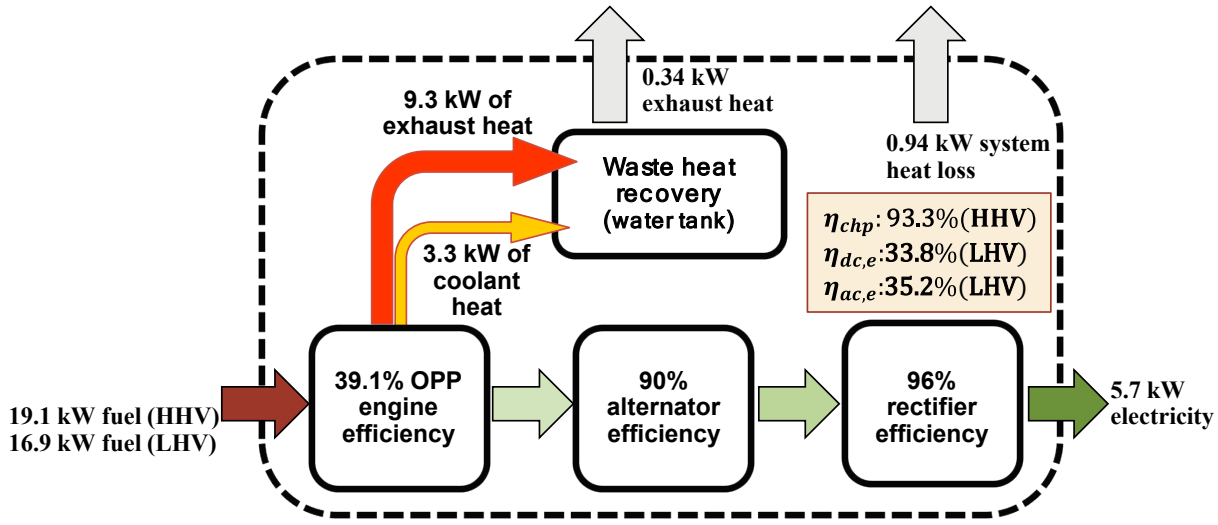

Figure 16. Energy flow and efficiencies for mCHP component and system with waste heat recovered and stored in the water tank. The mCHP operated at lean combustion mode.

5. LONG-DURATION TEST

An automatic testing system (shown in Figure 17) consisting of electrical battery and load emulator was established to connect the mCHP prototype in response to emulate any electrical load demand profile. In the system, the battery module delivers electricity to the electronic load bank in the load demand emulator. The mCHP control module manages mCHP operation by monitoring the battery voltage. The mCHP runs the engine and generates power if the battery voltage drops below the lower battery voltage boundary and turns off the engine once the battery voltage is above the upper battery voltage boundary. To minimize the potential damage of frequent engine on/off operation, each engine on/off cycle consists of four phases: engine warm-up mode, engine load cycle, engine cooldown mode, and engine shutdown.

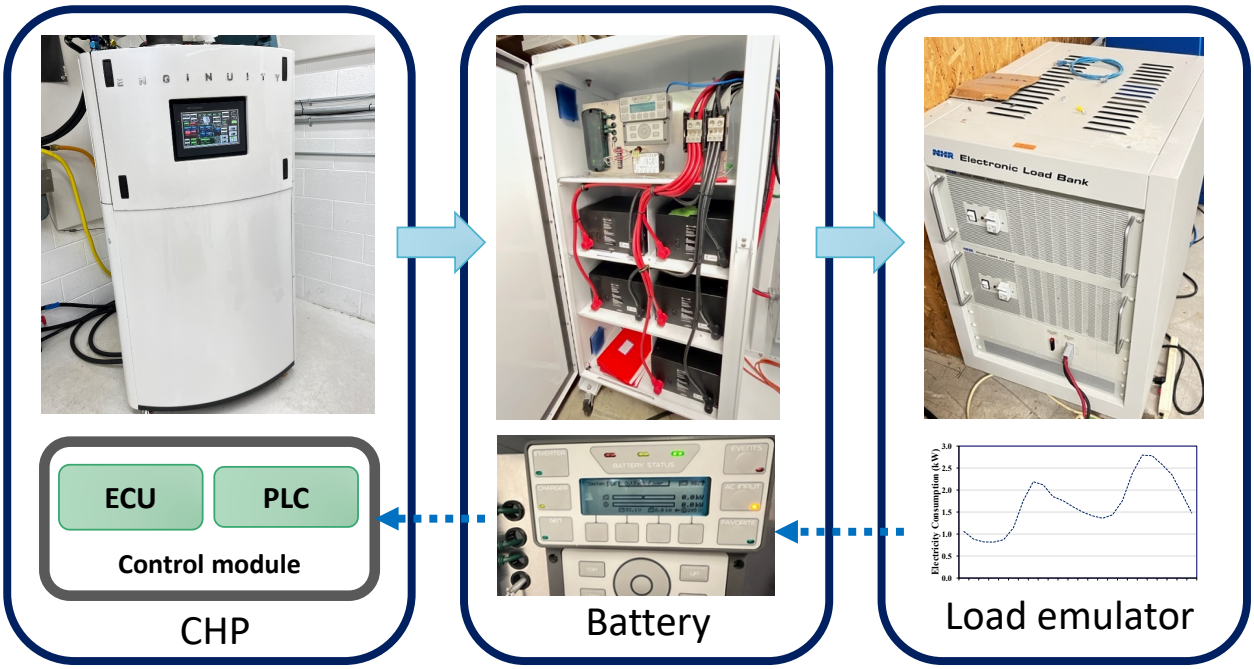

Figure 17. Automatic electrical load testing system: (a) the developed mCHP prototype, (b) 19kWh electrical battery, and (c) Transient load demand emulator.

In the long-duration test, the mCHP prototype was operated in the stoichiometric combustion mode and was tested in 24hr automatic operation mode, in which a 24-hr electrical load profile measured from a representative single-family house in New Jersey was implemented in the electrical load demand emulator. The grid was disconnected for this test. The battery was fully charged to 56.3 V at the beginning of the automatic test. The mCHP control module manages the battery voltage between 52.8 and 55.6 V, while maintaining average tank temperature of 60°C. To maintain tank water temperature, the hot water was pumped out and regular city water was added when the mCHP turned on. The details are shown in the supplemental document.

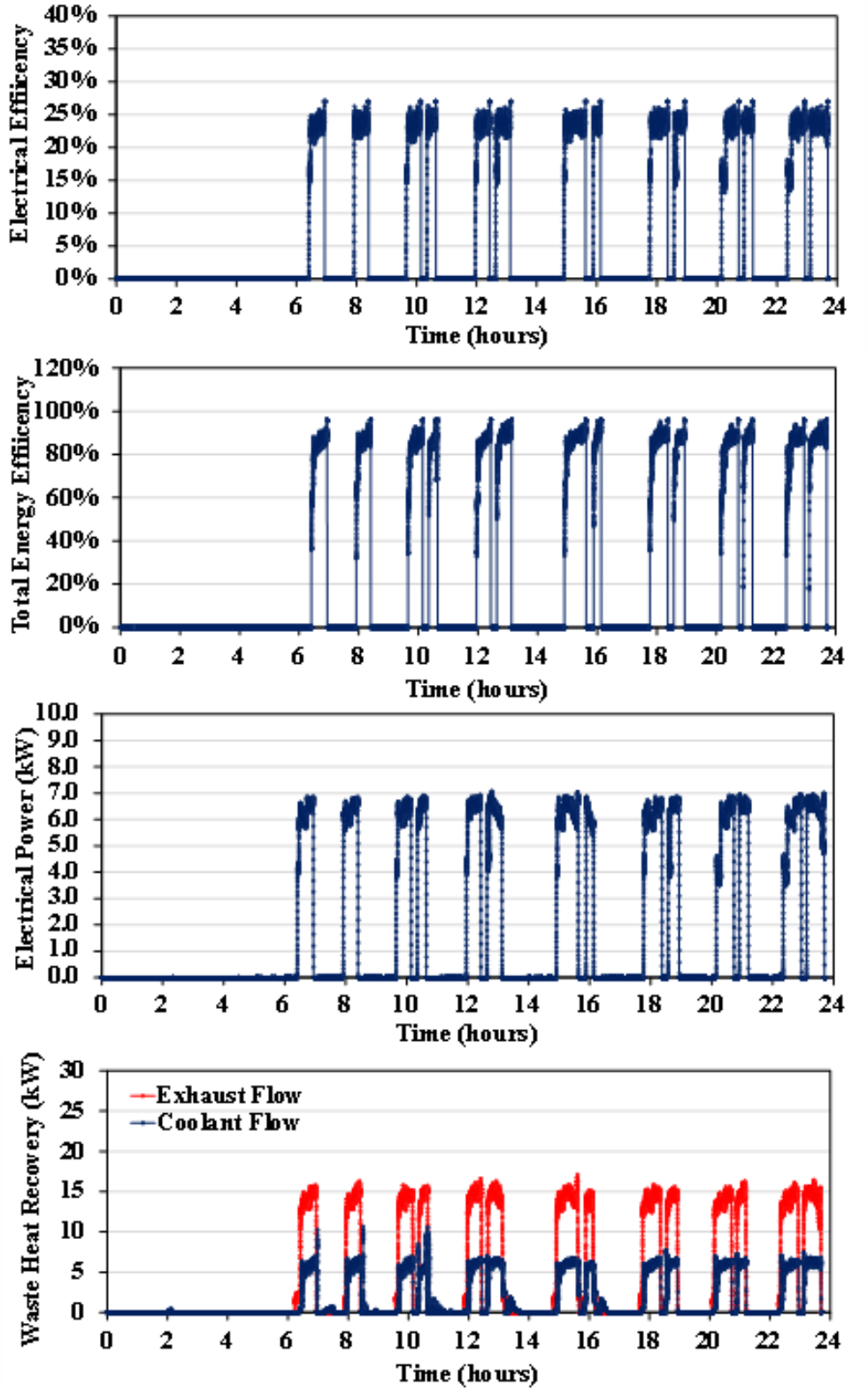

Figure 18. The 24-h automatic operation of the mCHP prototype at the rate of 6.5 kW. (a) Electrical efficiency, (b) overall mCHP energy efficiency, (c) electrical power generated by the mCHP, and (d) waste heat recovery from exhaust and coolant flows.

Figure 18 shows the performance of the mCHP prototype at the rate of 6.5 kW. During the first 6 h, the fully charged battery in the testing system provides requested electrical load in the simulated load profile and maintains mCHP water tank temperature via DC heater, as shown Figure 5. Then, the mCHP frequently turned on to charge the battery and to provide thermal energy to meet the thermal demand from hot water dumping and cold water filling. The data show that the unit achieved 23.1% of AC electricity efficiency (or 22.2% of DC electricity efficiency) and 84.2% of the overall mCHP efficiency over the 24-h mCHP operation. Moreover, the observation reveals that the 24-hr operation did not degrade any performance of the mCHP. This result indicates good potential of mCHP reliability and durability.

6. CONCLUSION

A novel mCHP prototype powered by an opposed-piston four-stroke engine, i.e. OP4S, was developed to provide heat and electricity simultaneously to single-family houses or light commercial buildings. Compared with conventional ICEs, the OP4S is simpler and cheaper to manufacture, assemble, and operate. OP4S also enable higher efficiency with less heat loss. The OP4S can use renewable gas (biogas), natural gas, propane, as well as hydrogen, to generate mechanical power and waste heat in the form of hot coolant and exhaust gas. In the mCHP, waste heat from the OP4S is efficiently recovered by using coolant flow circuit and exhaust gas coil. To enable efficient engine operation and proper lubrication, the developed mCHP includes a thermostat to maintain a returning coolant temperature of around 70°C–80°C to the engine by on splitting the coolant flow from the engine into two separate streams. The recovered thermal energy is stored in a 52 gal water tank and can be used as a domestic hot water supply as well as potential space heating application.

The power outputs of the mCHP prototype operated under the stoichiometric modes were tested in the range of 3.2–7.4 kW, and their AC electricity efficiencies vary between 16.8% and 26.4% and their DC electricity efficiencies are 16.1%–25.3%. The results reveal that larger electric power output leads to higher electric efficiency, whether waste heat is recovered and stored in the water tank or external thermal load is applied for hot water supply and space heating. The results further display that the overall mCHP efficiency is up to 93.1%, and the overall mCHP efficiency in all the cases is above 80%. Furthermore, the 24 h operation under the stoichiometric mode did not degrade any performance of the mCHP, indicating good potential of the prototype reliability and durability.

The lean combustion modes enable more than 30% improvement in energy efficiency. The maximum AC efficiency of the lean combustion mode enables to achieve 35.2%, and the engine efficiency is approaches 40%. The exceptional electrical efficiency breaks the typical upper boundary of 30% for ICE-based CHP. The engine exhaust temperatures in the lean modes are substantially less than in the stoichiometric modes. Moreover, the lean cases achieve high overall mCHP efficiencies: the overall mCHP efficiencies are all greater than 93%. The phenomenon may be due to less exhaust heat loss in the lean modes. Nearly 40% of electrical efficiency is expected in the proposed mCHP for the cases of 6.0 kW if technology can be applied to improve hardware limitations are overcome.

The mCHP prototype can achieve low-cost, with flexible matching of thermal and electrical loads while reducing the complexity of distribution and installation, along with high efficiency and its ability to use a variety of fuels, including biogas and hydrogen. The novel mCHP technology is expected to promote mCHP acceptance and accelerate the adoption of mCHP in the US residential and light commercial markets, given its compelling economics and drop-in replacement feature.

ACKNOWLEDGEMENTS

This work was sponsored by the US Department of Energy Office of Technology Transitions and Building Technologies Office with Antonio Bouza as a program manager. This research used resources at the Building Technologies Research and Integration Center, a US Department of Energy Office of Science User Facility operated by the Oak Ridge National Laboratory. The authors would like to thank several individuals at Enginuity Power Systems for their support and development of the base technology and hardware, most notably Dr. Abdullah Al Hadi, Nate Eifert, Greg Powell, Vince Meyers, Lara Reyes, and James Warren.

REFERENCES

1. Martinez S, Michaux G, Salagnac P, Bouvier J L. Micro-combined heat and power systems (micro-CHP) based on renewable energy sources. Energ Convers Manage 2017; 154: 262–285.
2. Caterpillar Inc. Combined Heat and Power. Cogeneration, https://www.cat.com/en_US/by-industry/electric-power/electric-power-industries/cogen-chp.html?&utm_content=epg_an_educational_epgasCHP&utm_source=google&utm_medium=cpc&utm_campaign=ep_gas_en_us_CHP_text&utm_term=combined_heat_and_power&gclid=CjwKCAjwtp2bBhAGEiwAOZZTuMtbbUNl3pSJ1Cw_itwLOtIDX9B0aSoxiZTOSZnlAAcZUvad4KuywxoCEOAQAvD_BwE; 2023 [accessed February 21, 2023].
3. Barbieri E S, Spina P R, Venturini M. Analysis of innovative micro-CHP systems to meet household energy demands. Appl Energ 2012; 97: 723–733.
4. Pepermans G, Driesen J, Haeseldonckx D, Belmans R, D'haeseleer W. Distributed generation: definition, benefits and issues. Energ Policy 2005; 33(6): 787–798.
5. Buffat R, Raubal M. Spatio-temporal potential of a biogenic micro CHP swarm in Switzerland. Renew Sust Energ Rev 2019; 103: 443–454.
6. Jung Y, Kim J, Lee H. Multi-criteria evaluation of medium-sized residential building with micro-CHP system in South Korea. Energ Buildings 2019; 193: 201–215.
7. Wu Q, Ren H, Gao W. Economic assessment of micro-CHP system for residential application in Shanghai, China. Energy Proced 2016; 88: 732–737.
8. Habibi M R, Varmazyar M. Comprehensive preliminary experimental performance investigation of a micro-CHP system by using an equipped test room. Appl Therm Eng 2018; 134: 428–436.
9. Caliano M, Bianco N, Graditi G, Mongibello L. Economic optimization of a residential micro-CHP system considering different operation strategies. Appl Therm Eng 2016; 101: 592–600.
10. Shaneb O A, Coates G, Taylor P C. Sizing of residential μCHP systems. Energ Buildings 2011; 43(8): 1991–2001.
11. Mohammadi H, Mohammadi M. Optimization of the micro combined heat and power systems considering objective functions, components and operation strategies by an integrated approach. Energ Conv Manage 2020; 208: 112610.
12. Giffin P K. Performance and cost results from a DOE Micro-CHP demonstration facility at Mississippi State University. Energ Conv Manage 2013; 65: 364–371.
13. De Paepe M, D'Herdt P, Mertens D. Micro-CHP systems for residential applications. Energ Conv Manage 2006; 47(18–19): 3435–3446.
14. Barbieri E S, Dai Y J, Morini M, Pinelli M, Spina P R, Sun P, Wang R Z. Optimal sizing of a multi-source energy plant for power heat and cooling generation. Appl Therm Eng 2014; 71(2): 736–750.
15. Kim C K, Yoon J Y. Performance analysis of bladeless jet propulsion micro-steam turbine for micro-CHP (combined heat and power) systems utilizing low-grade heat sources. Energy 2016; 101: 411–420.
16. Qiu G, Shao Y, Li J, Liu H, Riffat S B. Experimental investigation of a biomass-fired ORC-based micro-CHP for domestic applications. Fuel 2012; 96: 374–382.
17. Qiu K, Hayden A C S. Implementation of a TPV integrated boiler for micro-CHP in residential buildings. Appl Energ 2014; 134: 143–149.
18. Taie Z, Hagen C. Experimental thermodynamic first and second law analysis of a variable output 1–4.5 kWe, ICE-driven, natural-gas fueled micro-CHP generator. Energ Conv Manage 2019; 180: 292–301.

19. Taie Z, West B, Szybist J, Edwards D, Thomas J, Huff S, Vishwanathan G, Hagen C. Detailed thermodynamic investigation of an ICE-driven, natural gas-fueled, 1 kWe micro-CHP generator. Energ Conv Manage 2018; 166: 663–673.
20. Bell M, Swinton M, Entchev E, Gusdorf J, Kalbfleisch W, Marchand R, Szadkowski F. Development of micro combined heat and power technology assessment capability at the Canadian Centre for Housing Technology. B-6010. Ottawa, Ontario, Canada. 2003.
21. Glenergy. Dachs—Mini CHP Combined Heat and Power Technical Specification, http://glenergy.ie/wp-content/uploads/2016/10/Dachs_-_Mini_CHP_Technical_specification.pdf; 2016 [accessed February 21, 2023].
22. SOLO Stirling 161. https://www.scribd.com/document/353312261/SOLO-Stirling-161; [accessed February 21 2023].
23. Thomas B. Benchmark testing of Micro-CHP units. Appl Therm Eng 2008; 28(16): 2049–2054.
24. Boait P J, Greenough R. Can fuel cell micro-CHP justify the hydrogen gas grid? Operating experience from a UK domestic retrofit. Energ Buildings 2019; 194: 75–84.
25. Zhu S, Yu G, Jongmin O, Xu T, Wu Z, Dai W, Luo E. Modeling and experimental investigation of a free-piston Stirling engine-based micro-combined heat and power system. Appl Energ 2018; 226: 522–533.
26. Zhao W, Li R, Li H, Zhang Y, Qiu S. Numerical analysis of fluid dynamics and thermodynamics in a Stirling engine. Appl Therm Eng 2021; 189: 116727.
27. Abani N, Chiang M, Thomas I, Nagar N, Zermeno R, Regner G. Developing a 55+ BTE Commercial Heavy-Duty Opposed-Piston Engine without a Waste Heat Recovery System. In; Heavy-Duty-, On- und Off-Highway-Motoren. Springer Vieweg, Wiesbaden; 2016, p. 292–310.
28. Moser S, Gainey B, Lawler B, Filipi Z. Thermodynamic Analysis of Novel 4-2 Stroke Opposed Piston Engine. 2021-24-0096. Warrendale, Pennsylvania: SAE International; 2021.
29. Pirault J P, Flint M. Opposed-piston engine renaissance power for the future. San Diego, California: Achates Power Inc, 2010.
30. Mazuro P, Kozak D. Experimental investigation on the performance of the prototype of aircraft Opposed-Piston engine with various values of intake pressure. Energ Conv Manage 2022; 269: 116075.
31. Crosse J. Under the skin: Why opposed-piston engines are returning to roads, https://achatespower.com/under-the-skin-why-opposed-piston-engines-are-returning-to-roads/; 2021 [accessed February 21 2023].
32. Serrano J R, García A, Monsalve-Serrano J, Martínez-Boggio S. High efficiency two stroke opposed piston engine for plug-in hybrid electric vehicle applications: Evaluation under homologation and real driving conditions. Appl Energ 2021; 282: 116078.
33. Regner G, Herold R E , Wahl M H , Dion E , Redon F, Johnson D, Callahan B J , McIntyre S. The achates power opposed-piston two-stroke engine: performance and emissions results in a medium-duty application. SAE International Journal of Engines 2011; 4(3): 2726–2735.
34. Zoldak P, Douvry-Rabjeau J. Development of a Gaseous Fueled Boosted Opposed-Piston Four Stroke (OP4S) Engine, https://www.gtisoft.com/wp-content/uploads/2022/10/2022-GTTC-US-Enginuity-Opposed-Piston-Four-Stroke-Engine.pdf; 2022 [ccessed February 21, 2023].
35. Zoldak,P, Douvry-Rabjeau, J, Zyada, A, Potential of a Hydrogen-Fueled Opposed Piston Four stroke (OP4S) Engine, Society of Automotive Engineers – WCX23, 2023-01-0408, 2023.
36. Griffiths D. The Doxford Engine: its Development and Decline. Transactions of the Newcomen Society 1994; 66(1): 27–51.
37. Lamas M I, Rodríguez C G, Rodríguez J D, Telmo J. Numerical analysis of several port configurations in the Fairbanks-Morse 38D8-1/8 opposed piston marine engine. Brodogradnja: Teorija i praksa brodogradnje i pomorske tehnike 2015; 66(1): 1–11.

38. Gęca M, Czyż Z, Sułek M. Diesel engine for aircraft propulsion system. Combustion Engines 2017; 169(2):7–13.
39. Gao Z, Curran SJ, Parks II JE, Smith DE, Wagner RM, Daw CS, Edwards KD, Thomas JF. Drive cycle simulation of high efficiency combustions on fuel economy and exhaust properties in light-duty vehicles. Appl Energ 2015; 157: 762–776.
40. Gao Z, Chakravarthy V K, Daw C S. Comparisons of the simulated emissions and fuel efficiencies of diesel and gasoline hybrid electric vehicles. P I Mech Eng D-J Aut 2011; 225(7): 944–959.
41. Gao Z, LaClair T J, Nawaz K, Wu G, Hao P, Boriboonsomsin K, Todd M, Barth M, Goodarzi A. Comprehensive powertrain modeling for heavy-duty applications: A study of plug-in hybrid electric bus. Energ Conv Manage 2022; 252: 115071.

APPENDIX A. PATENT, PUBLICATIONS AND MEDIA REPORTS

PUBLICATIONS

- Z Gao et.al. Advanced micro-CHP powered by opposed piston engine, In preparation.
- M Zhang et.al. Modeling and optimization of a novel thermal energy storage for recovering two waste heat sources from a micro–combined heat and power system, In preparation.

APPENDIX B. CARDA Final Report Certification

Final Report Certification
for
CRADA Number NFO-10-07946

Between

UT-Battelle, LLC

and

Warren Engine Company (Now named as Enginuity Power Systems)
(Participant)

Instructions:

Mark the appropriate statement in 1a or 1b below with an "X." Refer to the articles in the CRADA terms and conditions governing the identification and marking of Protected CRADA Information (PCI).

If no PCI is identified, the report will be distributed without restriction. If PCI is identified, the report distribution will be limited in accordance with the CRADA terms and conditions governing release of data. In all cases items 2 and 3 must be true. That is, the report cannot contain Proprietary Information and a disclosure must be filed prior to release of the report.

This certification may either be made by using this form or may be made on company letterhead if the Participant desires. A faxed copy of this completed form is acceptable.

The following certification is made for the subject final report:

1. (a) ☐ The final report contains information that qualifies as "Protected CRADA Information" (PCI). The PCI legend is printed on the report cover, and the PCI is clearly identified.

OR

(b) ☒ The final report does not contain "Protected CRADA Information." The "Approved for Public Release" legend is printed on the report cover.

2. The final report does not contain Proprietary Information.

3. By the signature below, the Participant has no objection to the public distribution of the final report due to patentable information.

For the Participant:

Jacques Beaudry-Losique
(Name)

CEO
(Title)

03/16/2023
(Date)

ORNL 851 (9/2007)